

CuClarabel: GPU Acceleration for a Conic Optimization Solver

Yuwen Chen¹, Danny Tse², Parth Nobel³, Paul Goulart¹, and Stephen Boyd³

¹Department of Engineering Science, University of Oxford, Oxford, UK

²Department of Computer Science, Stanford University, Stanford, CA

³Department of Electrical Engineering, Stanford University, Stanford, CA

November 4, 2025

Abstract

We present the GPU implementation of the general-purpose interior-point solver Clarabel for convex optimization problems with conic constraints. We introduce a mixed parallel computing strategy that processes linear constraints first, then handles other conic constraints in parallel. The GPU solver currently supports linear equality and inequality constraints, second-order cones, exponential cones, power cones and positive semidefinite cones of the same dimensionality. We demonstrate that integrating a mixed parallel computing strategy with GPU-based direct linear system solvers enhances the performance of GPU-based conic solvers, surpassing their CPU-based counterparts across a wide range of conic optimization problems. We also show that employing mixed-precision linear system solvers can potentially achieve additional acceleration without compromising solution accuracy.

1 Introduction

We consider the following convex optimization problem [1] with a quadratic objective and conic constraints:

$$\begin{aligned} & \text{minimize} && \frac{1}{2}x^T Px + q^T x \\ & \text{subject to} && Ax + s = b, \\ & && s \in \mathcal{K}, \end{aligned} \tag{P}$$

with respect to x, s and with parameters $A \in \mathbf{R}^{m \times n}$, $b \in \mathbf{R}^m$, $q \in \mathbf{R}^n$ and $P \in \mathbf{S}_+^n$ and variables $x \in \mathbf{R}^n, s \in \mathbf{R}^m$. For the rest of the paper, \mathbf{S}_+^n represents the cone of positive semi-definite matrices. The cone \mathcal{K} is a closed convex cone. The formulation (P) is very general and can model most conic convex optimization problems in practice. Examples include the optimal power flow problem in power systems [2], model predictive control in control [3, 4], limit analysis of engineering structures in mechanics [5], support vector machines [6] and lasso problems [7] in machine learning, statistics, and signal processing, and portfolio optimization in finance [8, 9]. Linear equality (zero cones) and inequality (nonnegative cones), second-order cone [10], and semidefinite cone [11] constraints have been long supported in standard conic optimization solvers, and support for exponential and power cone constraints was recently included in several state-of-the-art conic optimization solvers [12, 13, 14, 15]. The combination of these cones can represent many more elaborate convex constraints through the lens of disciplined convex programming [16, 17, 18].

The dual problem of (\mathcal{P}) is

$$\begin{aligned} & \text{maximize} && -\frac{1}{2}x^T Px - b^T z \\ & \text{subject to} && Px + A^T z = -q, \\ & && z \in \mathcal{K}^*, \end{aligned} \tag{\mathcal{D}}$$

with respect to x, z and where \mathcal{K}^* is the dual cone of \mathcal{K} . Solving \mathcal{P} and \mathcal{D} is equivalent to solving the Karush-Kuhn-Tucker (KKT) conditions when strong duality holds. On the other hand, the set of strongly primal infeasibility certificates for (\mathcal{P}) is

$$\mathbb{P} = \{z \mid A^T z = 0, z \in \mathcal{K}^*, \langle b, z \rangle < 0\}, \tag{1}$$

and the set of strongly dual infeasibility certificates is

$$\mathbb{D} = \{x \mid Px = 0, -Ax \in \mathcal{K}, \langle q, x \rangle < 0\}. \tag{2}$$

Finding an optimal solution with strong duality or detecting a strongly infeasible certificate can be unified into solving a linear complementarity problem with two additional slack variables $\tau, \kappa \geq 0$ [19], which can be reformulated to the following problem:

$$\begin{aligned} & \text{minimize} && s^T z + \tau \kappa \\ & \text{subject to} && \frac{1}{\tau} x^T Px + q^T x + b^T z = -\kappa, \\ & && Px + A^T z + q\tau = 0, \\ & && Ax + s - b\tau = 0, \\ & && (s, z, \tau, \kappa) \in \mathcal{K} \times \mathcal{K}^* \times \mathbf{R}_+ \times \mathbf{R}_+, \end{aligned} \tag{\mathcal{H}}$$

with respect to x, s, z, τ, κ . It is well-known that when $P = 0$, (\mathcal{H}) is the *homogenous self-dual embedding* [20] of (\mathcal{P}) , and the extension for $P \neq 0$ can be regarded as a *homogeneous embedding* for linear complementarity problems [21, 22]. Precisely, in our case (\mathcal{H}) is homogeneous but not self-dual. In [15] it is also shown that \mathcal{H} is always (asymptotically) feasible, and we can recover either an optimal solution or a strong infeasibility certificate of (\mathcal{P}) and (\mathcal{D}) , depending on the value of the optimal solution $(x^*, z^*, s^*, \tau^*, \kappa^*)$ to (\mathcal{H}) :

- i) If $\tau^* > 0$ then $(x^*/\tau^*, s^*/\tau^*)$ is an optimal solution to (\mathcal{P}) and $(x^*/\tau^*, z^*/\tau^*)$ is an optimal solution to (\mathcal{D}) .
- ii) If $\kappa^* > 0$ then at least one of the following holds:
 - (\mathcal{P}) is strongly infeasible and $z^* \in \mathbb{P}$.
 - (\mathcal{D}) is strongly infeasible and $x^* \in \mathbb{D}$.

The optimal solution τ^*, κ^* satisfy the complementarity slackness condition, *i.e.*, at most one of τ^*, κ^* is nonzero. The pathological case $\tau^* = \kappa^* = 0$ has been discussed in [19].

The *interior-point method* [23] is a popular choice for solving (\mathcal{H}) . However, it usually requires to factorize linear systems that are increasingly ill-conditioned. The time complexity of matrix factorization scales with respect to the fill-in that is closely related to nonzeros of the matrix and permutation strategies during factorization. It is thus time-consuming to solve large-scale conic optimization problems with interior-point methods.

1.1 Our contribution

We contribute a GPU-accelerated implementation of the general-purpose interior-point solver Clarabel [15], in Julia. This implementation supports cases where \mathcal{K} is a product of *atomic* cones: zero cones, nonnegative cones, second-order cones, exponential cones, power cones and positive semidefinite cones. We propose a *mixed parallel computing strategy* that parallelizes

computing for each type of cone, integrates the cuDSS [24] library for linear system solving, and supports *mixed-precision* linear system solves for moderate speed improvements. Furthermore, we evaluate our solver against others across a variety of conic optimization problems. Our implementation of CuClarabel is open-sourced on GitHub¹ and can be easily accessed through CVXPY [25].

1.2 Related work

Interior-point methods and solver development. The interior-point method [23] was first discovered by Dikin [26], and became more mainstream after the conception of Karmarkar’s method [27], a polynomial-time algorithm for linear programming, and Renegar’s [28] path following method. Interior-point methods are known for their ability to solve conic optimization problems to high precision, and is chosen as the default algorithm for many conic optimization solvers [12, 29, 15, 30, 31]. Common variations of the interior-point method include potential reduction methods and path-following methods.

Interior-point methods employ a Newton-like strategy to compute a search direction at every iteration. Unfortunately, the matrix factorization required to compute this direction which scales with the dimension of an optimization problem, rendering very large problems difficult to solve. Developing efficient interior-point methods on exotic cones directly is a promising research direction [30, 31] to alleviate this computational burden. Using exotic cones, we can represent equivalent problems with significantly fewer variables and exploit sparse structure within these exotic cones for efficient implementation of interior-point methods [29, 32, 33]. However, operations within an exotic cone can hardly be parallelized, while parallelism across heterogeneous cones of different dimensionalities will introduce significant synchronization delay.

GPU acceleration in optimization algorithms. GPUs are playing an increasingly significant role in scientific computing. In optimization, GPUs are used to run solvers based on first-order methods. For example, CuPDLP [34] is based on the popular PDHG algorithm [35], which requires only matrix multiplication and addition without the use of direct methods (*i.e.*, it is *factorization-free*). Solvers that require the solution to linear systems, like SCS [13] and CuOSQP [36], have relied on indirect iterative methods—such as the conjugate gradient (CG), the minimal residual (MINRES) [37], and the generalized minimum residual (GMRES) [38] methods—to solve these systems on GPUs. However, the linear systems solved in first-order methods are generally much better conditioned than those encountered in interior-point methods, where the linear systems become increasingly ill-conditioned as the iterations progress. As an interior-point method approaches higher precision, the number of iterations for each inner indirect linear solves increases significantly, which will eventually offset benefits of GPU parallelism and make GPU-based interior-point methods less preferable compared to CPU-based solvers with direct methods in overall computational time [39]. Recently, NVIDIA released the cuDSS package [40], which provides fast direct methods on GPUs for sparse linear systems. Previous work has integrated cuDSS in a nonlinear optimization solver, MADNLP [41], resulting in significant speed-up on large-scale problems compared to its CPU-based counterpart.

Mixed-precision methods. Mixed-precision, or multiprecision, methods [42, 43] have become progressively more popular due to their synergies with modern GPU architectures. For example, in lower-precision configuration one enjoys significant speedup in algorithms, as modern architectures have 32-bit implementations that are around twice as fast as their 64-bit counterparts [42, 44]. Mixed precision methods aim to capitalize on the computational benefits of

¹<https://github.com/oxfordcontrol/Clarabel.jl/tree/CuClarabel>

performing expensive operations in lower precision, while maintaining (or reducing the negative impact to) the superior numerical accuracy from higher precision. Classically, mixed-precision methods for direct (linear system solving) methods involve factorizing a matrix in lower precision, and then applying iterative refinement. In this approach, only the more expensive steps, such as the matrix factorizations and backsolves, are done in lower precision. Mixed-precision methods are used throughout scientific computing, with applications including BLAS operations [45], different linear system solvers such as Krylov methods (CG, GMRES) [43, 46, 47], solving partial differential equations [48], and training deep neural networks [48, 49, 50].

1.3 Paper outline

In §2, we review supported cones and discuss the interior point method used by Clarabel [15] for solving conic optimization problems. In §3, we outline how to implement parallel computation for cone operations and solve linear systems within our GPU solver. §4 details our numerical experiments. We detail the scaling matrices for each cone in §A.

2 Backgrounds

We first review supported cones in CuClarabel with the corresponding barrier functions, along with their dual cones. We then briefly sketch the main operations used by the Clarabel solver [15] to compute a solution to (\mathcal{P}) .

2.1 Supported cones

We support the following atomic cones in our GPU solver:

- The *zero cone*, defined as

$$\{0\}^n = \{x \in \mathbf{R}^n \mid x_i = 0, i = 1, \dots, n\}.$$

The dual cone of the zero cone is $(\{0\}^n)^* = \mathbf{R}^n$.

- The *nonnegative cone*, defined as

$$\mathbf{R}_+^n = \{x \in \mathbf{R}^n \mid x_i \geq 0, i = 1, \dots, n\}.$$

The nonnegative cone is a self-dual convex cone, *i.e.*, $(\mathbf{R}_+^n)^* = \mathbf{R}_+^n$.

- The *second-order cone* $\mathcal{K}_{\text{soc}}^n$ (also called the *quadratic* or *Lorentz cone*), defined as

$$\mathcal{K}_{\text{soc}}^n = \{(t, x) \mid x \in \mathbf{R}^{n-1}, t \in \mathbf{R}_+, \|x\|_2 \leq t\}.$$

The second-order cone is self-dual, *i.e.*, $\mathcal{K}_{\text{soc}} = \mathcal{K}_{\text{soc}}^*$.

- The *positive semidefinite cone* $\mathcal{K}_{\text{psd}}^n$ is defined as

$$\mathcal{K}_{\text{psd}}^n = \{X \in \mathbb{S}^n \mid X \succeq 0\},$$

where \mathbb{S}^n denotes the space of $n \times n$ symmetric matrices, and $X \succeq 0$ indicates that X is positive semidefinite. The positive semidefinite cone is self-dual, *i.e.*, $\mathcal{K}_{\text{psd}}^n = (\mathcal{K}_{\text{psd}}^n)^*$.²

²In the current solver implementation, all positive semidefinite (PSD) cones are restricted to have dimension at most 32, and all PSD cones within a given problem must share the same dimension.

- The *exponential cone*, a 3-dimensional cone defined as

$$\mathcal{K}_{\text{exp}} = \left\{ (x, y, z) \mid y > 0, y \exp\left(\frac{x}{y}\right) \leq z \right\} \cup \{(x, 0, z) \mid x \leq 0, z \geq 0\},$$

with its dual cone given by

$$\mathcal{K}_{\text{exp}}^* = \left\{ (u, v, w) \mid u < 0, -u \exp\left(\frac{v}{u}\right) \leq \exp(1)w \right\} \cup \{(0, v, w) \mid v \geq 0, w \geq 0\}.$$

- The 3-dimensional *power cone* with exponent $\alpha \in (0, 1)$, defined as

$$\mathcal{K}_{\text{pow}, \alpha} = \{(x, y, z) \mid x^\alpha y^{1-\alpha} \geq |z|, x \geq 0, y \geq 0\},$$

with its dual cone given by

$$\mathcal{K}_{\text{pow}, \alpha}^* = \left\{ (u, v, w) \mid \left(\frac{u}{\alpha}\right)^\alpha \left(\frac{v}{1-\alpha}\right)^{1-\alpha} \geq |w|, u \geq 0, v \geq 0 \right\}.$$

2.2 Interior point method

Solving the problem (\mathcal{H}) amounts to finding a root of the following nonlinear equations

$$G(x, z, s, \tau, \kappa) = \begin{bmatrix} 0 \\ s \\ \kappa \end{bmatrix} - \begin{bmatrix} P & A^T & q \\ -A & 0 & b \\ -q^T & -b^T & 0 \end{bmatrix} \begin{bmatrix} x \\ z \\ \tau \end{bmatrix} + \begin{bmatrix} 0 \\ 0 \\ \frac{1}{\tau} x^T P x \end{bmatrix} = 0, \quad (3)$$

$(x, z, s, \tau, \kappa) \in \mathcal{F},$

where $\mathcal{F} := \mathbf{R}^n \times \mathcal{K}^* \times \mathcal{K} \times \mathbf{R}_+ \times \mathbf{R}_+$ defines the region of cone constraints. Besides the zero cone that is a linear constraint, other supported conic constraints are smoothed by nonlinear equations in pairs within an interior-point method,

$$s = -\mu \nabla f(z), \quad \tau \kappa = \mu, \quad (4)$$

where μ is the smoothing parameter and $f(\cdot)$ is the logarithmically homogeneous self-concordant barrier (LHSCB) function for cone \mathcal{K}^* . The barrier functions for different cones are:

1. *Nonnegative cone* \mathbf{R}_+^n of degree n :

$$f(z) = -\sum_{i \in [n]} \log(z_i), \quad z \in \mathbf{R}_+^n. \quad (5)$$

2. *Second order cone* \mathcal{K}_q^n of degree 1:

$$f(z) = -\frac{1}{2} \log\left(z_1^2 - \sum_{i=2}^n z_i^2\right), \quad z \in \mathcal{K}_q^n. \quad (6)$$

3. *Positive semidefinite cone* $\mathcal{K}_{\text{psd}}^n$ of degree n :

$$f(X) = -\log \det(X), \quad X \in \mathcal{K}_{\text{psd}}^n. \quad (7)$$

4. *Dual exponential cone* $\mathcal{K}_{\text{exp}}^*$ of degree 3:

$$f(z) = -\log\left(z_2 - z_1 - z_1 \log\left(\frac{z_3}{-z_1}\right)\right) - \log(-z_1) - \log(z_3), \quad z \in \mathcal{K}_{\text{exp}}^*. \quad (8)$$

5. *Dual power cone* $\mathcal{K}_{\text{pow}}^*$ of degree 3:

$$f(z) = -\log\left(\left(\frac{z_1}{\alpha}\right)^{2\alpha}\left(\frac{z_2}{1-\alpha}\right)^{2(1-\alpha)} - z_3^2\right) - (1-\alpha)\log(z_1) - \alpha\log(z_2), \quad z \in \mathcal{K}_{\text{pow}}^*. \quad (9)$$

The trajectory (also called the *central path*)

$$\begin{aligned} G(v) &= \mu G(v^0), \\ s &= -\mu \nabla f(z), \quad \tau \kappa = \mu, \end{aligned} \quad (10)$$

where $v = (x, z, s, \tau, \kappa)$, characterizes the solution of (3) in the right limit $\mu \rightarrow 0^+$, given an initial point v^0 . After starting from v^0 , the Clarabel solver iterates the following steps for each iteration k :

Update residuals and check the termination condition. We update several key metrics at the start of each iteration. Defining the normalized variables $\bar{x} = x/\tau$, $\bar{s} = s/\tau$, $\bar{z} = z/\tau$, the primal and dual residuals are then

$$\begin{aligned} r_p &= -A\bar{x} - \bar{s} + b, \\ r_d &= P\bar{x} + A^T\bar{z} + q, \\ g_p &= \frac{1}{2}\bar{x}^T P\bar{x} + q^T\bar{x}, \\ g_d &= -\frac{1}{2}\bar{x}^T P\bar{x} - b^T\bar{z} \end{aligned} \quad (11)$$

and complementarity slackness $\mu = \frac{s^T z + \kappa \tau}{\nu + 1}$, where ν is the degree of cone \mathcal{K} . The solver returns an approximate optimal point if

$$\begin{aligned} \|r_p\|_\infty &< \epsilon_{\text{feas}} \max\{1, \|b\|_\infty + \|\bar{x}\|_\infty + \|\bar{s}\|_\infty\} \\ \|r_d\|_\infty &< \epsilon_{\text{feas}} \max\{1, \|q\|_\infty + \|\bar{x}\|_\infty + \|\bar{z}\|_\infty\} \\ |g_p - g_d| &< \epsilon_{\text{feas}} \max\{1, \min\{|g_p|, |g_d|\}\}. \end{aligned} \quad (12)$$

Otherwise, it returns a certificate of primal infeasibility if

$$\begin{aligned} \|A^T z\|_\infty &< -\epsilon_{\text{inf}} \max(1, \|x\|_\infty + \|z\|_\infty)(b^T z) \\ b^T z &< -\epsilon_{\text{inf}}, \end{aligned} \quad (13a)$$

and a certificate of dual infeasibility if

$$\begin{aligned} \|Px\|_\infty &< -\epsilon_{\text{inf}} \max(1, \|x\|_\infty)(b^T z) \\ \|Ax + s\|_\infty &< -\epsilon_{\text{inf}} \max(1, \|x\|_\infty + \|s\|_\infty)(q^T x) \\ q^T x &< -\epsilon_{\text{inf}}. \end{aligned} \quad (13b)$$

Note that $\epsilon_{\text{feas}}, \epsilon_{\text{inf}}$ are predefined parameters within the Clarabel solver.

Find search directions. We then compute Newton-like search directions using a linearization of the central path (10). In other words, we solve the following linear system given some right-hand side residual $d = (d_x, d_z, d_\tau, d_s, d_\kappa)$,

$$\begin{bmatrix} 0 \\ \Delta s \\ \Delta \kappa \end{bmatrix} - \begin{bmatrix} P & A^T & q \\ -A & 0 & b \\ -(q + 2P\xi)^T & -b^T & \xi^T P\xi \end{bmatrix} \begin{bmatrix} \Delta x \\ \Delta z \\ \Delta \tau \end{bmatrix} = - \begin{bmatrix} d_x \\ d_z \\ d_\tau \end{bmatrix} \quad (14a)$$

$$H\Delta z + \Delta s = -d_s, \quad \kappa\Delta\tau + \tau\Delta\kappa = -d_\kappa, \quad (14b)$$

where $\xi = x\tau^{-1}$, and H is the same positive-definite scaling matrix as in the CPU version of Clarabel [15], also described in §A. We have shown in [15] that solving (14) reduces to solve the next linear system with two different right-hand sides,

$$\underbrace{\begin{bmatrix} P & A^T \\ A & -H \end{bmatrix}}_K \begin{bmatrix} \Delta x_1 & | & \Delta x_2 \\ \Delta z_1 & | & \Delta z_2 \end{bmatrix} = \begin{bmatrix} d_x & | & -q \\ -(d_z - d_s) & | & b \end{bmatrix}. \quad (15)$$

Since both P, H are positive semidefinite, adding a positive regularization to them makes K symmetric quasi-definite and thus strongly factorizable via the LDL^T decomposition [51]. After solving (15), we recover the search direction $\Delta = (\Delta x, \Delta z, \Delta \tau, \Delta s, \Delta \kappa)$ using

$$\begin{aligned} \Delta \tau &= \frac{d_\tau - d_\kappa/\tau + (2P\xi + q)^T \Delta x_1 + b^T \Delta z_1}{\kappa/\tau + \xi^T P \xi - (2P\xi + q)^T \Delta x_2 - b^T \Delta z_2} \\ &= \frac{d_\tau - d_\kappa/\tau + q^T \Delta x_1 + b^T \Delta z_1 + 2\xi^T P \Delta x_1}{\|\Delta x_2 - \xi\|_P^2 - \|\Delta x_2\|_P^2 - q^T \Delta x_2 - b^T \Delta z_2}, \end{aligned} \quad (16a)$$

and

$$\Delta x = \Delta x_1 + \Delta \tau \Delta x_2, \quad \Delta z = \Delta z_1 + \Delta \tau \Delta z_2, \quad (16b)$$

$$\Delta s = -d_s - H \Delta z, \quad \Delta \kappa = -(d_\kappa + \kappa \Delta \tau)/\tau. \quad (16c)$$

In an interior-point method with a predictor-corrector scheme, we need to solve (14) with two different values for d . The first is for the affine step (predictor) with

$$d = (G(x, z, s, \tau, \kappa), \kappa \tau, s). \quad (17)$$

The other assigns d as

$$\begin{aligned} (d_x, d_z, d_\tau) &= (1 - \sigma)G(x, z, s, \tau, \kappa), \quad d_\kappa = \kappa \tau + \Delta \kappa \Delta \tau - \sigma \mu, \\ d_s &= \begin{cases} W^T (\lambda \setminus (\lambda \circ \lambda + \eta - \sigma \mu \mathbf{e})) & \text{(symmetric)} \\ s + \sigma \mu \nabla f(z) + \eta & \text{(nonsymmetric)}, \end{cases} \end{aligned} \quad (18)$$

in the combined step (predictor+corrector), where $\lambda = W^{-T}s = Wz$ and \mathbf{e} is the idempotent for a symmetric cone with the product operator ‘ \circ ’ and its inverse operator ‘ \setminus ’ [52]. Here η denotes a higher-order correction term, which is a heuristic technique that can significantly accelerate the convergence of interior-point methods [53]. We set it to the Mehrotra correction [54]

$$\eta = (W^{-1} \Delta s) \circ (W \Delta z), \quad (19a)$$

for symmetric cones and the 3rd-order correction [55]

$$\eta = -\frac{1}{2} \nabla^3 f(z) [\Delta z^a, \nabla^2 f(z)^{-1} \Delta s^a], \quad (19b)$$

for nonsymmetric cones. The centering parameter σ controls the rate at which both the residual $G(x, z, s, \tau, \kappa)$ and the complementarity measure μ decrease. It is determined heuristically based on the value of the affine step size α_a , defined as the maximal step size ensuring that $v + \alpha_a \Delta_a \in \mathcal{F}$. Computing α_a is non-trivial in the presence of exponential and power cones. As a practical alternative, we perform a backtracking line search with a shrinking ratio of 0.8 to determine a feasible α_a for power and exponential cones.

Update iterates. At the end of each iteration k , we move the current iterate v along the combined direction $\Delta_c := (x, z, s, \tau, \kappa)$ and obtain the new iterate $v + \alpha_c \Delta_c$. As discussed, the combined step size α_c should satisfy $v + \alpha_c \Delta_c \in \mathcal{F}$. Furthermore, we must ensure that the new iterate $v + \alpha_c \Delta_c$ stays in the neighborhood $\mathcal{N}(\beta)$ of the central path (10) [55],

$$\mathcal{N}(\beta) = \{(s, z) \in \mathcal{K} \times \mathcal{K}^* \mid \nu_i \langle \nabla f^*(s_i), \nabla f(z_i) \rangle^{-1} \geq \beta \mu, i = 1, \dots, p\}, \quad (20)$$

where β is set to 10^{-6} .

3 GPU formulation of Clarabel

3.1 A primer on GPU programming

Originally developed for computationally demanding gaming applications, graphics processing units (GPUs) are *massively parallel, multithreaded, manycore processors*, with massive computational power and memory bandwidth. As a result, GPUs are used throughout scientific computing. In this section, we outline some core properties of GPU computing devices to highlight why a GPU implementation is a natural extension to Clarabel. We then discuss our specific implementation details.

Due to their natural parallelism, GPUs differ dramatically from CPUs in the way their transistors are configured. GPUs have a smaller number of caches (blocks where memory access is fast) and instruction processing blocks, and far more, albeit simpler, computational blocks (*i.e.*, arithmetic logic and floating point units). This suggests that CPUs utilize their larger caches to minimize instruction and memory latency within each thread, while GPUs switch between their significantly larger number of threads to hide said latency.

GPUs use a *single instruction, many threads* (SIMT) approach. In practice, the GPU receives a stream of instructions – each instruction is sent to groups of GPU cores (also known as a *warp*) and acts on multiple data in parallel. Each group of GPU cores, as a result, has *single instruction, many data* (SIMD) structure. This contrasts the traditional CPU vector lane approach of *single instruction, single data*. Note that modern CPUs also support SIMD, but at a much smaller scale than GPUs, as implied by the transistor layout. Furthermore, the SIMD structure requires data parallelism for parallel execution on a GPU.

3.2 GPU implementation for interior point method

We detail our GPU implementation of the primal-dual interior point method in Algorithm 1, which is divided into two phases: setup and solve. The setup phase involves data equilibration and solver initialization, while the solve phase implements the classical primal-dual interior point method. Synchronization is required at the end of each step in Algorithm 1.

The matrix factorization (step 5) and the back-solve (steps 6 and 9) are the most time-consuming parts in each iteration of an interior point method, and can be computed using the cuDSS package. Variable and information update (steps 11 and 12) contain matrix addition and multiplication operations that have already been supported in CUDA. Steps 4, 6, 7, 9, and 10 include cone operations that should be tailored for each cone, but we can abstract them into the same framework for parallelism. We will detail how to parallelize each of these steps under a unified framework in the next subsection.

Algorithm 1 Primal-dual interior-point method

Require: Parameter inputs P, A, q, b and cone information \mathcal{K} .

```
//Setup phase
1: Equilibrate  $P, A, q, b$ .
2: Initialize solver structure  $s$ , including matrix  $K$  and cuDSS solver.

//Solve phase
3: while termination check (12) or (13) is not satisfied do
4:   Update the scaling matrix  $H$  as in Appendix A.
5:   Factorize the matrix  $K$  in (15).
6:   Compute the right-hand residual  $d$  (17) for the affine step and solve (15) to obtain  $\Delta_a$ 
   via (16).
7:   Compute the affine step  $\alpha_a$  satisfying  $v + \alpha_a \Delta_a \in \mathcal{F}$ .
8:   Compute the centering parameter  $\sigma = (1 - \alpha_a)^3$ .
9:   Compute the right-hand residual  $d$  (18) for the combined step and solve (15) to obtain  $\Delta_c$ 
   via (16).
10:  Compute the combined step  $\alpha_c$  satisfying  $v + \alpha_c \Delta_c \in \mathcal{F}$  with the neighborhood check.
11:  Update the variable  $v \leftarrow v + 0.99\alpha_c \Delta_c$ .
12:  Update residuals and objective values in (11).
13: end while
```

3.3 Mixed parallel computing strategy

The cone operations related to steps 4, 6, 7, 9, and 10 above require only information local to each constituent cone, and hence can be executed concurrently with respect to individual cones. We propose the *mixed parallel computing strategy* for a cone operation across different types of cones. Each family of cones is handled in parallel, and families of cones can be addressed by separate streams.

As stated earlier, the cone operations related to zero cones and nonnegative cones are simply vector additions and multiplications, which have already been parallelized in CUDA. In our implementation we aggregate all zero cones into a single zero cone in our preprocessing step. The same holds for nonnegative cones. For the remaining cones, we parallelize within each *family* of cones (*i.e.*, second-order cone, exponential cone, etc.). For each family of cones, we allocate a thread to each cone belonging to that family, and execute in parallel. This adheres to the SIMD computing paradigm, as each type of cone has its own set of instructions for updating its scaling matrix.

We employ our mixed parallel computing strategy in step 4, the scaling matrix update. Recall that the conic constraint \mathcal{K} can be decomposed as a Cartesian product of p constituent atomic cones $\mathcal{K}_1 \times \cdots \times \mathcal{K}_p$ that are ordered by cone types. We assume \mathcal{K}_1 is a zero cone, \mathcal{K}_2 is a nonnegative cone, \mathcal{K}_3 to \mathcal{K}_i are second-order cones, \mathcal{K}_{i+1} to \mathcal{K}_j are exponential cones, \mathcal{K}_{j+1} to \mathcal{K}_l are power cones and \mathcal{K}_{l+1} to \mathcal{K}_p are positive semidefinite cones. Due to our decomposition into constituent atomic cones, H is a block-diagonal matrix,

$$H = \begin{bmatrix} H_1 & & \\ & \ddots & \\ & & H_p \end{bmatrix},$$

where H_1 and H_2 are diagonal matrices and each block $H_t, t \geq 3$ is the scaling matrix corresponding to cone \mathcal{K}_t of small dimensionality.

Algorithm 2 illustrates the update of scaling matrix H^k in function `_update_H(v^k)`. For the

Algorithm 2 Algorithmic sketch for the scaling matrix H^k update in Algorithm 1

Require: Current iterate v^k , streams $st_{soc}, st_{exp}, st_{pow}, st_{sdp}$.

```
1: function _update_H( $v^k$ )
2:   Update  $H_{zero}^k$  // Zero cone ( $t = 1$ )
3:   Update  $H_{nn}^k$  // Nonnegative cone ( $t = 2$ )
4:
5:   // Second-order cones
6:    $H_{soc}^k = \text{\_kernel\_soc\_update\_H}<st_{soc}>()$  //  $t = 3$  to  $i$ 
7:
8:   // Exponential cones
9:    $H_{exp}^k = \text{\_kernel\_exp\_update\_H}<st_{exp}>()$  //  $t = i + 1$  to  $j$ 
10:
11:  // Power cones
12:   $H_{pow}^k = \text{\_kernel\_pow\_update\_H}<st_{pow}>()$  //  $t = j + 1$  to  $l$ 
13:
14:  // Positive semidefinite cones
15:   $H_{sdp}^k = \text{\_kernel\_sdp\_update\_H}<st_{sdp}>()$  //  $t = l + 1$  to  $p$ 
16:
17:  // Synchronize scaling update
18:  CuDeviceSynchronize()
19:
20:  return  $H^k$  // Output the scaling matrix  $H^k$ 
21: end
```

update of H at iteration k , we first set diagonal terms of the scaling matrix H_1^k for the zero cone to all 0s, and then update the diagonals of the scaling matrix H_2^k for the nonnegative cone by element-wise vector division, as in the Nesterov-Todd (NT) scaling [56]. These computations are already parallelized by CUDA. For conic constraints other than the zero cone and the nonnegative cone, the corresponding parts in the scaling matrix H are no longer diagonal, but we observe H_t only requires local information within each constituent cone, and thus we can solve for each H_t concurrently, independent to the other cones. We implement kernel functions `_kernel_soc_update_H()`, `_kernel_exp_update_H()`, `_kernel_pow_update_H()` and `_kernel_sdp_update_H()` for second-order cones, exponential cones, power cones and positive semidefinite cones respectively. Details regarding the update functions for each type of cone can be found in §A. Each kernel function will process one cone per thread, and updating scaling matrices of the same class of cones is executed in parallel. Kernel functions for different cone classes are launched independently in separate streams. Synchronization is required at the end of the scaling matrix update.

Since the mixed parallel computing strategy is independent of choices of optimization algorithms, it is also applicable for GPU implementations for cone operations in first-order operator-splitting conic solvers, like SCS [13] and COSMO [14].

Note that the SIMD GPU computing structure naturally favors *balanced workloads*, *i.e.*, the workloads in each thread should be similar so that the synchronization will not take too much time. The exponential and power cones are 3-dimensional nonsymmetric cones that all cone operations have balanced workload among the same class of cones, thus we can parallelize the computation for each cone. On the other hand, the second-order cones may vary in dimensionality, which may not mesh well with the SIMD computing paradigm. In most use cases for large-scale second-order cone problems, *e.g.*, optimal power flow problems [2] and finite-element problems [5], the second-order cones are of small (less than 5) dimensionality; thus the effect of

this workload imbalance is negligible. Regardless, we support second-order cones of all sizes. In the next section, we outline how to process second-order cones of high dimensionality.

3.4 Dynamic parallelism for second-order cones

Due to the definition of the barrier function (6) over a second-order cone $(t, x) \in \mathcal{K}_q^n$, the computation of residuals involving $t^2 - \|x\|^2$ requires substantial reduction operations within each cone. This introduces an additional level of parallelism, particularly relevant when the dimension of a second-order cone reaches thousands or more, as seen in applications like multistage portfolio optimization.

In such high-dimensional cases, processing second-order cones in a purely thread-wise fashion above becomes inefficient, as the residual computation becomes effectively single-threaded. A straightforward workaround is to use the dot product operations provided by cuBLAS for computing residuals. However, this approach processes each high-dimensional cone sequentially and fails to exploit cone-level parallelism when multiple second-order cones are present. To address this, we implement custom reduction operations and leverage *dynamic parallelism* in CUDA, which enables additional cone-level parallelism and better utilization of GPU resources.

Algorithm 3 illustrates how to compute q residuals via dynamic parallelism. Suppose we have a vector $x := [x_1; \dots; x_q]$ where $x_i := (t_i, u_i) \in \mathcal{K}_q^{n_i}$ and residual vector $r \in \mathbf{R}^q$ that stores the residual of cone i , *i.e.*, $r[i] = t_i^2 - \|u_i\|^2$. We first launch `_parent_kernel_soc_residual(x, r)` for the residual computation. We then launch q child kernel functions, `_child_kernel_soc_residual(x_i, r)`, for each thread i ($1 \leq i \leq q$) within the parent kernel function, processing the residual of cone i . The 2-norm of u_i can be realized by the standard parallel reduction utilizing shared memory efficiently, see Algorithm 4. Finally, we obtain the residual for each cone i and store it back to r in the child function.

Algorithm 3 Dynamic parallelism for the residual computation of q second-order cones

Require: $x = [x_1; x_2; \dots; x_q]$ and $r \in \mathbf{R}^q$, where $x_i = [t_i; u_i] \in \mathbf{R}^{n_i+1}$

```

1:
2: // Parent function
3: function _parent_kernel_soc_residual(x, r)
4:      $i \leftarrow (\text{blockIdx.x} - 1) * \text{blockDim.x} + \text{threadIdx.x}$  // Julia is 1-indexed
5:     if ( $i \leq q$ )
6:          $x_i \leftarrow$  extract cone block  $i$  from  $x$ 
7:
8:         //compute residual of each cone  $i$ 
9:         _child_kernel_soc_residual(x_i, r)
10:    end
11: end
12:
13: // Child function
14: function _child_kernel_soc_residual(x_i, r)
15:      $t_i \leftarrow x_i[1]$  // Julia: 1-based indexing
16:      $u_i \leftarrow x_i[2 : \text{end}]$ 
17:      $\|u\|_2^2 \leftarrow$  _reduction_norm2(u_i, n_i)
18:      $r[i] \leftarrow t_i^2 - \|u_i\|_2^2$ 
19: end

```

3.5 Batched support for positive semidefinite cones

The positive semidefinite (PSD) cone is a matrix cone that can vary in dimensionality. Computing scaling matrices and step sizes involves several matrix factorizations, such as Cholesky factorization, singular value decomposition and eigenvalue decomposition [52]. In CuClarebel, we address this by using batched matrix factorizations provided by the cuSOLVER library. Hence, we only support a restricted class of SDPs in which all PSD cones have the same dimensionality that is less than or equal to 32. This includes examples from finite element analysis problems [57, 58], where each SDP constraint encodes localized, element-wise or point-wise conditions—such as stress admissibility or yield criteria—that can be uniformly applied across the mesh.

3.6 Data structures

Since data parallelism is required for parallel execution on GPUs, we manage data for each cone as a structure of arrays (SoA) in our GPU implementation, in contrast to the existing CPU counterpart which uses an array of structures (AoS). In other words, instead of creating structs for $\mathcal{K}_i, i = 1, \dots, p$ and storing pointers to each struct in an array, we concatenate the same type of local variable from different cones into a global variable and then store it in a global struct for \mathcal{K} , which is illustrated in Figure 1.

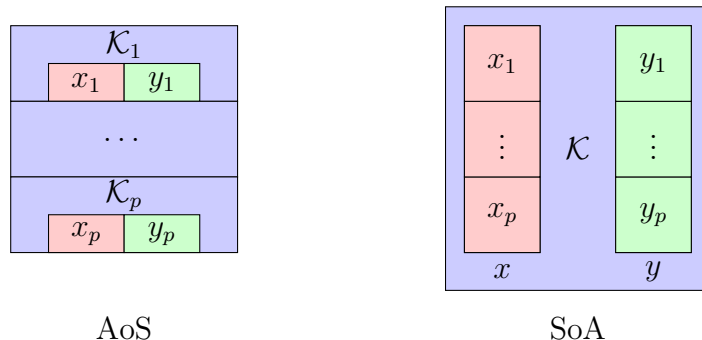


Figure 1: Illustration of AoS (CPU) and SoA (GPU) data structure

In addition, indexing cones in order in the setup phase can simplify the implementation of mixed parallel computing strategy. We reorder the input cones such that memory is coalescing for the same class of cones, which can accelerate computation on GPUs. Matrices are stored in the compressed sparse row (CSR) format. Instead of storing only the triangular part of a square matrix as in the CPU-based Clarebel, we store the full matrix for more efficient multiplication on the GPU.

3.7 Solving linear systems

Most of the computation time for our interior point method is spent in factorizing the matrix K and in the three backsolve operations in (15). Our GPU implementation also leverages the power of the newly released sparse linear system solver cuDSS [40] for the LDL^T factorization and backsolve operations. We implement a self-contained iterative refinement originated from [59] to increase the numerical stability of the backsolve operation.

Currently, a GPU has more computing cores for FLOAT32 than FLOAT64 and hence better performance for parallel algorithms. Also, FLOAT32 requires less memory and takes less time for the same computation than FLOAT64. However, lowering the precision will introduce numerical instability for solving linear systems. Thus, we employ a *mixed precision* solve in our matrix solves. Specifically, we use mixed precision for data within the iterative refinement step:

1. Solve for the residual at step i : $r_i = b - Kx_{i-1}$, where x_{i-1} is our guess for iteration $i - 1$. (Full precision)
2. Solve the linear system under a regularization parameter $(K + \delta I)\Delta_i = r_i$. (Lower precision)
3. Take $x_i = x_{i-1} + \Delta_i$. (Full precision)

In all our matrix solves, given matrix K and right-hand side b , we factorize the lower precision copy of K , and then solve the linear system in this lower precision. To enhance numerical stability during matrix factorization, a regularization term δI with

$$\delta := \delta_s + \delta_d \max_i |D_{ii}|,$$

is added to K , where δ_s is a static regularization and $\delta_d \max_i |D_{ii}|$ provides dynamic scaling based on the magnitude of the diagonal entries of D . To offset the regularization effect and rounding errors from the lower precision in backsolves, we solve in full precision for the other steps, *i.e.*, we compute the residual r_i and save the update $\{x_i\}$ in full precision. When we change the factorization data type from FLOAT32 to FLOAT64, it reduces down to the standard iterative refinement as employed in standard conic optimization solvers [15, 29].

We apply iterative refinement until either (1) we reach a pre-specified number of max steps T_{\max} for iterative refinement, or (2) the ℓ_∞ norm of $b - Kx_i$ reaches a certain threshold, specifically $\|b - Kx_i\|_\infty \leq t_{\text{abs}} + t_{\text{rel}} \|b\|_\infty$. We set both t_{abs} (absolute tolerance) and t_{rel} (relative tolerance) to 10^{-12} , and the maximum number of steps $T_{\max} = 10$. We set δ_s to the square root of machine precision, *i.e.*, $\sqrt{\epsilon} \approx 3.45e^{-4}$, for mixed precision and $\delta_s = 1e^{-8}$ for full precision, and we set δ_d to the square of machine precision, *i.e.*, ϵ^2 .

Although the mixed precision for the iterative refinement can improve the numerical stability for solving linear system in lower precision, it is to be expected that the mixed precision may take longer time to converge or fail in cases where the matrix K is extremely ill-conditioned. Caution is required when using mixed precision for numerically hard problems, *e.g.*, conic programs with exponential cones. Hence, we provide the mixed precision as an optional choice and use FLOAT64 by default.

4 Numerical experiments

We have benchmarked our Julia GPU implementation of the Clarabel solver, denoted as *Clarabel-GPU*, against the state-of-the-art commercial interior-point solvers MOSEK [12] and Gurobi [60]. We also include our Rust CPU implementation of Clarabel solver with the 3rd-party multi-threaded supernodal LDL factorization method in the *faer-rs* package [61], denoted as *ClarabelRs*. Note that MOSEK and Gurobi already utilize multithreaded linear system solvers. We include benchmark results for several classes of problems including quadratic programming (QP), second-order cone programming (SOCP) and exponential cone programming. All benchmarks are performed using the default settings for each solver, with pre-solve disabled where applicable to ensure equivalent problem-solving conditions. No additional iteration limits are imposed beyond each solver's internal defaults. We set $\epsilon_{\text{feas}} = 1e^{-6}$ for all solvers in termination check.

All experiments were carried out on a workstation with Intel(R) Xeon(R) w9-3475X CPU @ 4.8 GHz with 256 GB RAM and NVIDIA GeForce RTX 4090 24GB GPU. All benchmarks tests are scripted in Julia and access solver interfaces via JuMP [82]. We use Rust compiler version 1.76.0 and Julia version 1.10.2. Before recording benchmark tests, we run a few example solves; this offsets the just-in-time (JIT) precompilation overhead in Julia.

4.1 Benchmarking metrics

We choose the same benchmarking tests as used in the Clarabel solver [15], and compare our results using metrics that are commonly used when comparing computational time across different solvers. For a set of N test problems, we define the *shifted geometric mean* g_s as

$$g_s = \left[\prod_{p=1}^N (t_{p,s} + k) \right]^{\frac{1}{N}} - k,$$

where $t_{p,s}$ is the time in seconds for solver s to solve problem p , and $k = 1$ is the shift. The normalized shifted geometric mean is then defined as

$$r_s = \frac{g_s}{\min_{s'} g_{s'}}.$$

Note that the solver with the lowest shifted geometric mean solve time has a normalized score of 1. We assign a solve time $t_{p,s}$ equal to the maximum allowable solve time if solver s fails to solve the problem p .

The *relative performance ratio* for a solver s and a problem p is defined as

$$u_{p,s} = \frac{t_{p,s}}{\min_{s'} t_{p,s'}}.$$

The *relative performance profile* denotes the fraction of problems solved by solver s within a factor τ of the solve time of the best solver, which is defined as $f_s^r : \mathbf{R}_+ \mapsto [0, 1]$

$$f_s^r(\tau) = \frac{1}{N} \sum_p \mathcal{I}_{\leq \tau}(u_{p,s}),$$

where $\mathcal{I}_{\leq \tau}(u) = 1$ if $\tau \leq u$ and $\mathcal{I}_{\leq \tau}(u) = 0$ otherwise. For $\tau = 1$, $f_s^r(1)$ denotes the ratio of problems where the solver s performs the best, and $\sum_s f_s^r(1)$ should be equal to 1 if every problem is solvable for at least one solver. We also compute the *absolute performance profile* $f_s^a : \mathbf{R}_+ \mapsto [0, 1]$, which denotes the fraction of problems solved by solver s within τ seconds and is defined as

$$f_s^a(\tau) = \frac{1}{N} \sum_p \mathcal{I}_{\leq \tau}(t_{p,s}).$$

Our numerical experiments highlight the performance gains achieved by the GPU implementation of Clarabel on a diverse set of conic optimization problems. We record *total time* by default, the sum of the *setup time*, including data equilibration and solver initialization, and the *solve time*, which is the running time for the algorithm underlying a solver.

4.2 Quadratic programming

We first present benchmark results for QPs. Note that in this setting, the set \mathcal{K} in (\mathcal{P}) is restricted to the composition of zero cones, *i.e.*, linear equality constraints, and nonnegative

cones, *i.e.*, linear inequality constraints. We consider two classes of problems, the portfolio optimization problem and the Huber fitting problem.

Portfolio optimization, a problem arising in quantitative finance, aims to allocate assets in a manner that maximizes expected return while keeping risk under control. We can formulate it as

$$\begin{aligned} & \text{maximize} && \mu^T x - \gamma x^T \Sigma x \\ & \text{subject to} && \mathbf{1}^T x = 1, \\ & && x \geq 0, \end{aligned}$$

where $x \in \mathbf{R}^n$ (the variable) represents the ratio of allocated assets, $\mu \in \mathbf{R}^n$ is the vector of expected returns, $\gamma > 0$ is the risk-aversion parameter, and $\Sigma \in \mathbf{S}_+^n$ the risk covariance matrix which is of the form $\Sigma = FF^T + D$ with $F \in \mathbf{R}^{p \times n}$ and $D \in \mathbf{R}^{p \times p}$ diagonal. We set the rank p to the integer closest to $0.1n$, and vary n from 5000 to 25000.

Huber fitting is a version of robust least squares. For a given matrix $A \in \mathbf{R}^{m \times n}$ and vector $b \in \mathbf{R}^m$, we replace the least squares loss function with the Huber loss. The Huber loss makes the penalty incurred by larger points linear instead of quadratic, thus outliers have a smaller effect on the resulting estimator. Precisely, the problem is stated as:

$$\text{minimize} \quad \sum_{i=1}^m \phi_h(a_i^T x - b_i)$$

where a_i^T is the i -th row of A and the Huber loss $\phi_h : \mathbf{R} \rightarrow \mathbf{R}$ is defined as

$$\phi_h(t) = \begin{cases} t^2 & |t| \leq T \\ T(2|t| - T) & \text{otherwise} \end{cases}.$$

We set m to the nearest integer of $1.5n$ and vary value of n from 5000 to 25000.

Table 1: Benchmarking for quadratic programming

Problem	iterations				total time (s)			
	ClarabelGPU	Mosek*	ClarabelRs	Gurobi	ClarabelGPU	Mosek*	ClarabelRs	Gurobi
PORTFOLIO_OPTIMIZATION_5000	15	9	15	16	0.372	0.936	7.36	0.513
PORTFOLIO_OPTIMIZATION_10000	18	10	18	17	1.42	4.24	48.8	2.8
PORTFOLIO_OPTIMIZATION_15000	18	11	18	17	3.55	12.7	147	7.52
PORTFOLIO_OPTIMIZATION_20000	17	12	17	17	6.66	28.5	307	14.7
PORTFOLIO_OPTIMIZATION_25000	18	11	18	18	11.8	49.3	549	27.2
HUBER_FITTING_5000	8	11	8	9	4.81	13.5	65.6	48.2
HUBER_FITTING_10000	8	11	8	9	37.1	55.1	612	276
HUBER_FITTING_15000	8	13	8	10	122	289	2.1e+03	747
HUBER_FITTING_20000	8	13	-	10	283	807	-	1.76e+03
HUBER_FITTING_25000	8	15	-	10	547	1.83e+03	-	1.24e+03

Results for large QP tests are shown in Table 1. We benchmark ten different examples from two classes above and set the time limit to 1h. We compare our GPU implementation ClarabelGPU with ClarabelRs and two commercial solvers, Gurobi and MOSEK. ClarabelGPU is the fastest solver on these problems, and it has the lowest per-iteration time for almost all examples. Since most of time of an interior point solver is spent on factorizing and solving a linear system in QPs, we can say that ClarabelGPU benefits from the use of the cuDSS linear system solver and it is more than 2 times faster than Gurobi, about 4 times faster than MOSEK and 10x times faster than the existing Rust implementation with the multithreaded *faer-rs* linear system solver.

4.3 Second-order cone programming

We next consider the second-order cone relaxations of optimal power flow problems [62] from the IEEE PLS PGLib-OPF benchmark library [2], using the *PowerModels.jl* package [63] for modeling convenience. Note that only second-order cones of dimensionality 3 or 4 are used in these

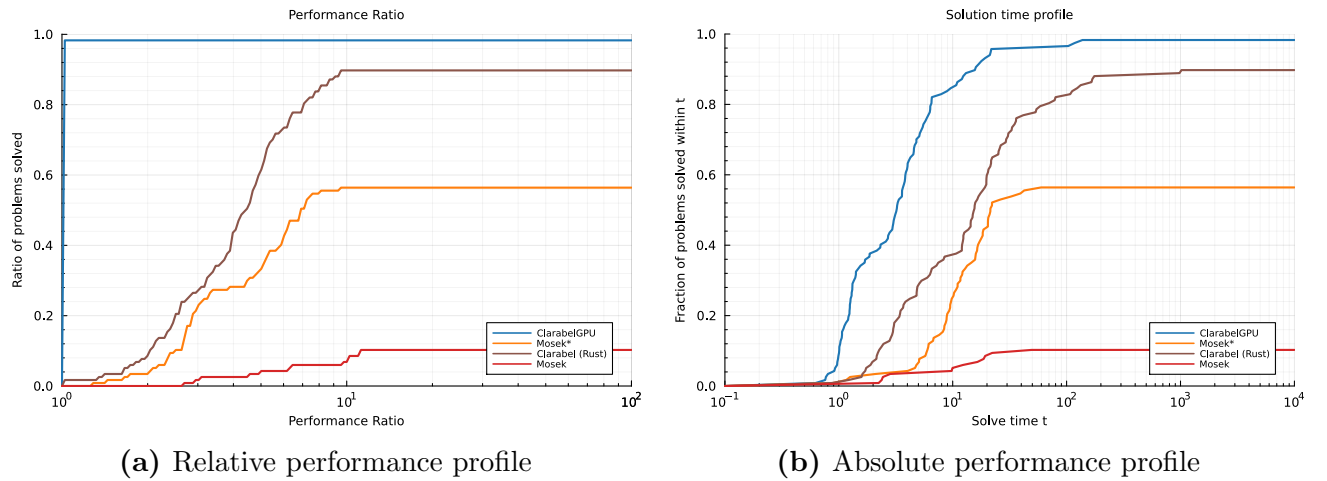
second-order cone relaxations, which satisfies our assumption in §3.3: that the dimensionality of each cone is very small.

We compare our GPU implementation with the CPU-based Clarabel solver and MOSEK solver. We also include results of the MOSEK solver with pre-solve for comparison, which is denoted as **Mosek*** in the plots. The maximum termination time is again set to 1h. We benchmark the second-order cone relaxations of 120 problems from the PGLib-OPF library, where the number of second-order cones exceed 2000.

Results for these problems are shown in Figure 2. Both ClarabelGPU and ClarabelRs are faster and more numerically stable than MOSEK even with the presolve step. Moreover, the GPU implementation can solve 118 out of 120 examples within an hour, while the Rust version of Clarabel can solve 104 out of 120 examples within the same time limit. In contrast, MOSEK with presolve fails on about 40% of the optimal flow problems, and the one without presolve fails on over 90% of the problems.

Overall, the GPU solver is several times faster than Rust-based CPU solver. This speedup causes ClarabelGPU to achieve a lower failure rate than ClarabelRs as it could solve more problems in under 10^4 seconds each. However, note that ClarabelGPU fails on two examples that ClarabelRs successfully solves. This highlights the different numerical performance of the linear system solvers between cuDSS and *faer-rs*.

Figure 2: Performance profiles for the large OPF SOCPs problem set



		ClarabelGPU	Mosek*	ClarabelRs	Mosek
Shifted GM	Full Acc.	1.0	12.12	4.59	53.65
	Low Acc.	1.0	4.16	3.91	7.29
Failure Rate (%)	Full Acc.	1.7	43.6	10.3	89.7
	Low Acc.	0.0	5.1	1.7	0.9

(c) Benchmark timings as shifted geometric mean and failure rates

We also consider the following multistage portfolio optimization problem:

$$\begin{aligned}
& \text{minimize} && \sum_{t=1}^T (-\mu_t^\top x_t + c \cdot \mathbf{1}^\top z_t + \gamma \cdot r_t) \\
& \text{subject to} && z_1 \geq x_1 - x_0, \quad z_1 \geq x_0 - x_1, \\
& && z_t \geq x_t - x_{t-1}, \quad z_t \geq x_{t-1} - x_t, \quad \forall t = 2, \dots, T, \\
& && \mathbf{1}^\top x_1 = d + \mathbf{1}^\top x_0, \quad \mathbf{1}^\top x_t = \mathbf{1}^\top x_{t-1}, \quad \forall t = 2, \dots, T, \\
& && y_t = F_t x_t, \quad \forall t = 1, \dots, T, \\
& && \begin{bmatrix} r_t \\ U y_t \\ D_{\text{sqr}} \odot x_t \end{bmatrix} \in \mathcal{K}_q^{n+k+1}, \quad \forall t = 1, \dots, T,
\end{aligned} \tag{21}$$

with respect to x , y , z , and r . This problem is formulated over T time periods, allocating wealth across n assets while managing exposure to k underlying factors. Here, x_t represents asset allocations, y_t represents factor exposures, z_t represents trade volumes, and r_t is a risk proxy. We impose additional constraints $x_t \in [0, 0.1]^n$, $y_t \in [0, 0.1]^k$, $z_t \in \mathbb{R}^n$, and $r_t \geq 0$. Our objective is a minimization over the trade-off between negative expected returns, linear transaction costs, and a second-order cone-based risk penalty scaled by risk aversion γ . The transaction constraints ensure that trade volumes z_t correctly reflect changes in portfolio weights. Budget constraints enforce capital conservation: initial capital changes by a known inflow d , and total capital remains constant thereafter. Factor exposure is modeled via linear mappings $y_t = F_t x_t$. Risk r_t is quantified through a second-order cone (SOC) constraint that captures both systematic risk $U y_t$ and idiosyncratic risk $D_{\text{sqr}} \odot x_t$ across each time period.

We benchmark multistage portfolio optimization problems with $n = 5000$, $k = 50$ and varying horizon T in Table 2; ClarabelGPU achieved up to a 3x speedup over MOSEK and 40x over ClarabelRs.

Table 2: Multi-stage portfolio optimization with varying horizons

Horizon	iterations				total time (s)			
	ClarabelGPU	Mosek*	ClarabelRs	Mosek	ClarabelGPU	Mosek*	ClarabelRs	Mosek
5	21	15	21	14	0.882	1.24	12.1	1.65
10	22	15	22	15	1.79	3.87	53.7	4.63
15	22	14	22	12	2.8	7.49	99.5	7.42
20	22	15	22	11	3.91	12.5	167	13.2
25	24	18	24	14	9.82	20.2	245	19.8
30	23	12	23	13	11.3	22.1	312	28

4.4 Exponential cone programming

For exponential programming, we benchmark the entropy maximization problems [13] with varying dimensionality. The entropy maximization problem aims to maximize entropy over a probability distribution given a set of m linear inequality constraints, which can be interpreted as bounds on the expectations of arbitrary functions. The problem is formulated as

$$\begin{aligned}
& \text{maximize} && -\sum_{i=1}^n x_i \log x_i \\
& \text{subject to} && \mathbf{1}^\top x = 1, \\
& && Ax \leq b,
\end{aligned}$$

Each element of A is generated from the distribution $A_{ij} \sim \mathcal{N}(0, n)$. Then, we set $b = Av/1^T v$ where $v \in \mathbf{R}^n$ is generated randomly from $v_i \sim U[0, 1]$, which ensures the problem is always feasible. We set m to the nearest integer of $0.5n$ and vary value of n from 2000 to 10000.

Table 3: Benchmarking for exponential cone programming

Problem	iterations				total time (s)			
	ClarabelGPU	Mosek*	ClarabelRs	Mosek	ClarabelGPU	Mosek*	ClarabelRs	Mosek
ENTROPY_MAX_2000	20	15	20	10	0.476	0.794	2.84	0.609
ENTROPY_MAX_4000	20	16	20	9	1.4	3.02	14	2.28
ENTROPY_MAX_6000	21	16	21	9	3.16	8.85	90.5	5.89
ENTROPY_MAX_8000	21	16	21	10	5.98	17.7	104	12.1
ENTROPY_MAX_10000	21	16	23	10	19.2	31.6	239	36.5

The benchmark results for these two problems with varying dimensionality are shown in Table 3. Though the GPU acceleration of Clarabel is offset by nearly doubled number of iterations compared to MOSEK, we can still achieve more than 2 times of acceleration for the overall time. That is to say we can possibly achieve more acceleration in ClarabelGPU if we can improve the numerical stability to the same level of MOSEK on exponential cone programs. We find ClarabelGPU can benefit from GPU computation up to 10x times faster compared to ClarabelRs.

4.5 Semidefinite programming

Our results in Table 4 show that ClarabelGPU achieves a speedup of $1.5\times$ to $4\times$ over MOSEK, both with and without presolve, and up to $10\times$ speedup compared to ClarabelRs. ClarabelGPU can only solve FELA_SDP_9263 to $1e^{-5}$ precision and is less numerical stable than Mosek* under the default setting, but increasing the static regularization δ_s to $1e^{-7}$ can fix the numerical issue.

Table 4: FEM with 3×3 -dimensional SDP constraints

Problem	iterations				total time (s)			
	ClarabelGPU	Mosek*	ClarabelRs	Mosek	ClarabelGPU	Mosek*	ClarabelRs	Mosek
FELA_SDP_1048	23	24	-	22	2.41	6.75	-	2.84
OBEFM_SDP_1048	19	13	19	15	2.48	5.98	30.6	4.04
FELA_SDP_4444	30	31	-	38	11	40.8	-	19.4
OBEFM_SDP_4444	20	13	20	-	11.5	35.3	144	-
FELA_SDP_9263	-	33	31	34	-	55.1	167	41.5
OBEFM_SDP_9263	21	14	21	-	25.4	38.1	323	-

4.6 Parametric programming

Clarabel supports updating the coefficients P, A, q, b without reinitializing the solver object. This feature is particularly advantageous for parametric programming, where the solver setup is required only once, and the symbolic factorization structure can be reused efficiently in subsequent solves [64]. Such capability is especially useful in applications like model predictive control and portfolio optimization.

For the multistage portfolio optimization problem in (21), we also split the total time into two parts, the setup time and the solve time, and report the ratio of them respectively in Table 5. Notably, the setup time for ClarabelGPU constitutes a larger proportion of the total time compared to its CPU counterpart. This suggests that, when the setup time dominates the total computational time, higher acceleration ratios can be achieved on a GPU when we need to solve multistage portfolio optimization multiple times with different parameters.

Table 5: Time ratio between setup and solve time on multistage portfolio optimization

Horizon	ClarabelGPU		Clarabel	
	setup time	solve time	setup time	solve time
5	0.648	0.352	0.418	0.582
10	0.654	0.346	0.36	0.64

Table 5: Time ratio between setup and solve time on multistage portfolio optimization

Horizon	ClarabelGPU		Clarabel	
	setup time	solve time	setup time	solve time
15	0.662	0.338	0.321	0.679
20	0.651	0.349	0.284	0.716
25	0.475	0.525	0.242	0.758
30	0.566	0.434	0.223	0.777

4.7 Mixed precision

In the implementation of the mixed precision setting, as described we only set the data type of the cuDSS linear system solver to `FLOAT32`. Since the use of mixed precision accelerates the numerical factorization rather than the symbolic factorization within a factorization method, we only record the computational time for an interior point method without the setup time.

We test the mixed precision setting on QPs, including portfolio optimization and Huber fitting problems from §4.2, for high accuracy level $\epsilon_{\text{feas}} = 1e^{-8}$. We compare it with the standard GPU implementation of `FLOAT64` data type. The results in Table 6 demonstrate that employing a mixed-precision strategy can reduce solve time by up to a factor of 2 when the matrix A becomes dense. However, we note that mixed precision is less numerically stable when solving an ill-conditioned KKT system (15). This can lead to an increased number of iterative refinement steps and longer solve times compared to full precision, or even failure to converge to the desired tolerance.

Table 6: Solve times and iteration counts for the mixed precision QP test

Problem	iterations		solve time (s)	
	Full	Mixed	Full	Mixed
PORTFOLIO_OPTIMIZATION_N_5000	17	18	0.18	0.29
PORTFOLIO_OPTIMIZATION_N_10000	19	19	0.70	0.57
PORTFOLIO_OPTIMIZATION_N_15000	19	19	1.8	1.31
PORTFOLIO_OPTIMIZATION_N_20000	19	23	3.74	3.26
PORTFOLIO_OPTIMIZATION_N_25000	19	21	6.79	5.58
HUBER_FITTING_N_5000	9	9	3.6	1.85
HUBER_FITTING_N_10000	10	10	36.9	19.9
HUBER_FITTING_N_15000	10	10	128	70.5
HUBER_FITTING_N_20000	9	9	279	156
HUBER_FITTING_N_25000	10	10	598	334

5 Conclusion

We have developed a GPU interior point solver for conic optimization.³ In our implementation, we propose a mixed parallel computing strategy to process linear constraints with second-order cone, exponential cone, power cone and semidefinite cone constraints. Our GPU solver shows several times acceleration compared to state-of-the-art CPU conic solvers on many problems to high precision, such as QPs, SOCPs, exponential cone programs and SDPs.

Future research directions include extending support to general SDPs with PSD cones of varying dimensionalities. The proposed mixed parallel computing strategy for GPU implementation is also applicable to conic solvers based on first-order operator-splitting methods. This approach could improve GPU utilization, especially when sufficient computational resources are available to handle different cone classes in parallel. Additional performance gains may be achieved through kernel fusion, the use of CUDA graphs to reduce kernel launch overhead and overlapping more independent computation within interior-point methods.

³<https://github.com/oxfordcontrol/Clarabel.jl/tree/CuClarabel>

Acknowledgments

Yuwen Chen was supported by the EPSRC Impact Acceleration Account Fund and the National Centre of Competence in Research (NCCR) Automation, funded by the Swiss National Science Foundation (SNSF). Parth Nobel was supported in part by the National Science Foundation Graduate Research Fellowship Program under Grant No. DGE-1656518. Any opinions, findings, and conclusions or recommendations expressed in this material are those of the author(s) and do not necessarily reflect the views of the National Science Foundation. The work of Stephen Boyd was supported by ACCESS (AI Chip Center for Emerging Smart Systems), sponsored by InnoHK funding, Hong Kong SAR.

References

- [1] Stephen Boyd and Lieven Vandenbergh. *Convex Optimization*. Cambridge University Press, 2004.
- [2] Sogol Babaeinejadsarookolae, Adam Birchfield, Richard Christie, Carleton Coffrin, Christopher DeMarco, Ruisheng Diao, Michael Ferris, Stephane Fliscounakis, Scott Greene, Renke Huang, et al. The power grid library for benchmarking AC optimal power flow algorithms. *arXiv:1908.02788*, 2019.
- [3] Francesco Borrelli, Alberto Bemporad, and Manfred Morari. *Predictive control for linear and hybrid systems*. Cambridge University Press, 2017.
- [4] Stephen Boyd, Laurent El Ghaoui, Eric Feron, and Venkataramanan Balakrishnan. *Linear Matrix Inequalities in System and Control Theory*. Society for Industrial and Applied Mathematics, 1994.
- [5] Athanasios Makrodimopoulos and Chris Martin. Upper bound limit analysis using simplex strain elements and second-order cone programming. *International Journal for Numerical and Analytical Methods in Geomechanics*, 31(6):835–865, 2007. eprint: <https://onlinelibrary.wiley.com/doi/pdf/10.1002/nag.567>.
- [6] Corinna Cortes and Vladimir Vapnik. Support-vector networks. *Machine Learning*, 20(3):273–297, 1995.
- [7] Robert Tibshirani. Regression shrinkage and selection via the Lasso. *Journal of the Royal Statistical Society: Series B*, 58(1):267–288, 1996.
- [8] Pavlo Krokmal. Higher moment coherent risk measures. *Quantitative Finance*, 7(4):373–387, 2007.
- [9] Alexander Vinel and Pavlo Krokmal. Certainty equivalent measures of risk. *Annals of Operations Research*, 249(1-2):75–95, 2017.
- [10] Miguel Sousa Lobo, Lieven Vandenbergh, Stephen Boyd, and Hervé Lebret. Applications of second-order cone programming. *Linear Algebra and its Applications*, 284(1):193–228, 1998. International Linear Algebra Society (ILAS) Symposium on Fast Algorithms for Control, Signals and Image Processing.
- [11] Lieven Vandenbergh and Stephen Boyd. Semidefinite programming. *SIAM Review*, 38(1):49–95, 1996.
- [12] MOSEK ApS. *MOSEK Modeling Cookbook*, 2023.

- [13] Brendan O’Donoghue, Eric Chu, Neal Parikh, and Stephen Boyd. Conic optimization via operator splitting and homogeneous self-dual embedding. *Journal of Optimization Theory and Applications*, 169(3):1042–1068, 2016.
- [14] Michael Garstka, Mark Cannon, and Paul Goulart. COSMO: A conic operator splitting method for convex conic problems. *Journal of Optimization Theory and Applications*, 190(3):779–810, 2021.
- [15] Paul Goulart and Yuwen Chen. Clarabel: An interior-point solver for conic programs with quadratic objectives, May 2024. arXiv:2405.12762 [math].
- [16] Michael Grant. *Disciplined Convex Programming*. PhD thesis, Stanford University, 2004.
- [17] Michael Grant and Stephen Boyd. CVX: Matlab software for disciplined convex programming, version 2.1. <https://cvxr.com/cvx>, March 2014.
- [18] Anqi Fu, Balasubramanian Narasimhan, and Stephen Boyd. CVXR: An R package for disciplined convex optimization. *Journal of Statistical Software*, 94(14):1–34, 2020.
- [19] Brendan O’Donoghue. Operator Splitting for a Homogeneous Embedding of the Linear Complementarity Problem. *SIAM Journal on Optimization*, 31(3):1999–2023, January 2021.
- [20] Yinyu Ye, Michael Todd, and Shinji Mizuno. An $o(\sqrt{nl})$ -iteration homogeneous and self-dual linear programming algorithm. *Mathematics of Operations Research*, 19(1):53–67, 1994.
- [21] Erling D. Andersen and Yinyu Ye. On a homogeneous algorithm for the monotone complementarity problem. *Mathematical Programming*, 84(2):375–399, 1999.
- [22] Akiko Yoshise. Interior point trajectories and a homogeneous model for nonlinear complementarity problems over symmetric cones. *SIAM Journal on Optimization*, 17(4):1129–1153, 2007.
- [23] Yurii Nesterov and Arkadii Nemirovskii. *Interior-Point Polynomial Algorithms in Convex Programming*. Society for Industrial and Applied Mathematics, 1994.
- [24] Cudss.jl: Julia interface for nvidia cudss, 2024. <https://github.com/exanauts/CUDSS.jl>.
- [25] Steven Diamond and Stephen Boyd. Cvxpy: A python-embedded modeling language for convex optimization, 2016.
- [26] Iliya Dikin. Iterative solution of problems of linear and quadratic programming. *Sov. Math., Dokl.*, 8:674–675, 1967.
- [27] Narendra Karmarkar. A new polynomial-time algorithm for linear programming. In *Proceedings of the Sixteenth Annual ACM Symposium on Theory of Computing*, STOC ’84, page 302–311, New York, NY, USA, 1984. Association for Computing Machinery.
- [28] James Renegar. A polynomial-time algorithm, based on newton’s method, for linear programming. *Math. Program.*, 40(1–3):59–93, jan 1988.
- [29] Alexander Domahidi, Eric Chu, and Stephen Boyd. ECOS: An SOCP solver for embedded systems. In *2013 European Control Conference (ECC)*, pages 3071–3076, 2013.
- [30] Chris Coey, Lea Kapelevich, and Juan Pablo Vielma. Solving natural conic formulations with Hypatia.jl. *INFORMS Journal on Computing*, 34(5):2686–2699, 2022.

- [31] Mehdi Karimi and Levent Tunçel. Domain-driven solver (DDS) version 2.1: a matlab-based software package for convex optimization problems in domain-driven form. *Mathematical Programming Computation*, 10 2023.
- [32] Martin Andersen, Joachim Dahl, and Lieven Vandenbergh. Implementation of nonsymmetric interior-point methods for linear optimization over sparse matrix cones. *Mathematical Programming Computation*, 2(3):167–201, 2010.
- [33] Yuwen Chen and Paul Goulart. An Efficient Implementation of Interior-Point Methods for a Class of Nonsymmetric Cones. *Journal of Optimization Theory and Applications*, 204(2):33, January 2025.
- [34] Haihao Lu and Jinwen Yang. cuPDLP.jl: A GPU Implementation of Restarted Primal-Dual Hybrid Gradient for Linear Programming in Julia, December 2023.
- [35] Antonin Chambolle and Thomas Pock. A First-Order Primal-Dual Algorithm for Convex Problems with Applications to Imaging. *Journal of Mathematical Imaging and Vision*, 40(1):120–145, May 2011.
- [36] Michel Schubiger, Goran Banjac, and John Lygeros. GPU Acceleration of ADMM for Large-Scale Quadratic Programming. *Journal of Parallel and Distributed Computing*, 144:55–67, October 2020. arXiv:1912.04263 [math].
- [37] Yousef Saad. *Iterative Methods for Sparse Linear Systems*. Other Titles in Applied Mathematics. Society for Industrial and Applied Mathematics, January 2003.
- [38] Youcef Saad and Martin Schultz. Gmres: A generalized minimal residual algorithm for solving nonsymmetric linear systems. *SIAM Journal on Scientific and Statistical Computing*, 7(3):856–869, 1986.
- [39] Edmund Smith, Jacek Gondzio, and Julian Hall. GPU Acceleration of the Matrix-Free Interior Point Method. In Roman Wyrzykowski, Jack Dongarra, Konrad Karczewski, and Jerzy Waśniewski, editors, *Parallel Processing and Applied Mathematics*, pages 681–689, Berlin, Heidelberg, 2012. Springer.
- [40] Nvidia Inc. CUDSS, 2023. <https://developer.nvidia.com/cudss>.
- [41] François Pacaud, Sungho Shin, Alexis Montoisson, Michel Schanen, and Mihai Anitescu. Condensed-space methods for nonlinear programming on GPUs, May 2024. arXiv:2405.14236 [math].
- [42] Ahmad Abdelfattah, Hartwig Anzt, Erik Boman, Erin Carson, Terry Cojean, Jack Dongarra, Mark Gates, Thomas Grützmacher, Nicholas Higham, Xiaoye Sherry Li, Neil Lindquist, Yang Liu, Jennifer A. Loe, Piotr Luszczek, Pratik Nayak, Srikara Pranesh, Sivasankaran Rajamanickam, Tobias Ribizel, Barry Smith, Kasia Swirydowicz, Stephen Thomas, Stanimire Tomov, Yaohung Tsai, Ichitaro Yamazaki, and Ulrike Meier Yang. A survey of numerical methods utilizing mixed precision arithmetic. *CoRR*, abs/2007.06674, 2020.
- [43] Nicholas Higham and Theo Mary. Mixed precision algorithms in numerical linear algebra. *Acta Numerica*, 31:347–414, 2022.
- [44] Marc Baboulin, Alfredo Buttari, Jack Dongarra, Jakub Kurzak, Julie Langou, Julien Langou, Piotr Luszczek, and Stanimire Tomov. Accelerating scientific computations with mixed precision algorithms. *CoRR*, abs/0808.2794, 2008.

- [45] Ahmad Abdelfattah, Timothy Costa, Jack Dongarra, Mark Gates, Azzam Haidar, Sven Hammarling, Nicholas Higham, Jakub Kurzak, Piotr Luszczek, Stanimire Tomov, and Mawussi Zounon. A set of batched basic linear algebra subprograms and lapack routines. *ACM Trans. Math. Softw.*, 47(3), June 2021.
- [46] Erin Carson and Tomáš Gergelits. Mixed precision s -step lanczos and conjugate gradient algorithms, 2021.
- [47] Serge Gratton, Ehouarn Simon, David Titley-Peloquin, and Philippe Toint. Exploiting variable precision in gmres, 2020.
- [48] Joel Hayford, Jacob Goldman-Wetzler, Eric Wang, and Lu Lu. Speeding up and reducing memory usage for scientific machine learning via mixed precision, 2024.
- [49] Paulius Micikevicius, Sharan Narang, Jonah Alben, Gregory Diamos, Erich Elsen, David Garcia, Boris Ginsburg, Michael Houston, Oleksii Kuchaiev, Ganesh Venkatesh, and Hao Wu. Mixed precision training, 2018.
- [50] Matthieu Courbariaux, Yoshua Bengio, and Jean-Pierre David. Training deep neural networks with low precision multiplications, 2015.
- [51] Robert Vanderbei. Symmetric quasidefinite matrices. *SIAM Journal on Optimization*, 5(1):100–113, 1995.
- [52] Lieven Vandenbergh. *The CVXOPT linear and quadratic cone program solvers*, 2010.
- [53] Stephen Wright. *Primal-Dual Interior-Point Methods*. Society for Industrial and Applied Mathematics, 1997.
- [54] Sanjay Mehrotra. On the Implementation of a Primal-Dual Interior Point Method. *SIAM Journal on Optimization*, 2(4):575–601, November 1992. Publisher: Society for Industrial and Applied Mathematics.
- [55] Joachim Dahl and Erling Andersen. A primal-dual interior-point algorithm for nonsymmetric exponential-cone optimization. *Mathematical Programming*, 2021.
- [56] Yurii Nesterov and Michael Todd. Primal-dual interior-point methods for self-scaled cones. *SIAM Journal on Optimization*, 8(2):324–364, 1998.
- [57] Christopher M. Martin and Athanasios Makrodimopoulos. Finite-element limit analysis of mohr–coulomb materials in 3d using semidefinite programming. *Journal of Engineering Mechanics*, 134(4):339–347, 2008.
- [58] Jyant Kumar and Debasis Mohapatra. Lower-bound finite elements limit analysis for hoek-brown materials using semidefinite programming. *Journal of Engineering Mechanics*, 143(9):04017077, 2017.
- [59] Jorge Nocedal and Stephen Wright. *Numerical Optimization*. Springer Series in Operations Research and Financial Engineering. Springer New York, New York, NY, 2006.
- [60] Gurobi Optimization, LLC. Gurobi Optimizer Reference Manual, 2023.
- [61] A linear algebra foundation for the Rust programming language. <https://github.com/sarah-ek/faer-rs>. Accessed: 2024-15-05.
- [62] Rabih Jabr. Radial distribution load flow using conic programming. *IEEE Transactions on Power Systems*, 21(3):1458–1459, Aug 2006.

- [63] Carleton Coffrin, Russell Bent, Kaarthik Sundar, Yeesian Ng, and Miles Lubin. Powermodels.jl: An open-source framework for exploring power flow formulations. In *2018 Power Systems Computation Conference (PSCC)*, pages 1–8, June 2018.
- [64] Martin Herceg, Michal Kvasnica, Colin Jones, and Manfred Morari. Multi-Parametric Toolbox 3.0. In *Proc. of the European Control Conference*, pages 502–510, 2013.
- [65] Levent Tunçel. Generalization of primal-dual interior-point methods to convex optimization problems in conic form. *Foundations of Computational Mathematics*, 1(3):229–254, 2001.

A Scaling matrices

The scaling matrix H in (14) is the Jacobian from the linearization of the central path (10). We set $H = 0$ for the zero cone and choose the NT scaling [56] for nonnegative and second-order cones, which are both symmetric cones. The NT scaling method exploits the self-scaled property of symmetric cone \mathcal{K} where exists a unique scaling point $w \in \mathcal{K}$ satisfying

$$H(w)s = z.$$

The matrix $H(w)$ can be factorized as $H^{-1}(w) = W^T W$, and we set $H = H^{-1}(w)$ in (14). The factors w, W are then computed following [52].

For exponential and power cones that are not symmetric, the central path is defined by the set of point satisfying

$$Hz = s, \quad H\nabla f^*(s) = \nabla f(z),$$

where f^* is the conjugate function of f , and the symmetric scaling from [65, 55] is implemented. We define *shadow iterates* as

$$\tilde{z} = -\nabla f(s), \quad \tilde{s} = -\nabla f^*(z),$$

with $\tilde{\mu} = \langle \tilde{s}, \tilde{z} \rangle / \nu$. A scaling matrix H is chosen to be the rank-4 Broyden-Fletcher-Goldfarb-Shanno (BFGS) update as in a quasi-Newton method,

$$H = H_{\text{BFGS}} = Z(Z^T S)^{-1} Z^T + H_a - H_a S (S^T H_a S)^{-1} S^T H_a,$$

where $Z = [z, \tilde{z}]$, $S = [s, \tilde{s}]$ and $H_a = \mu \nabla^2 f(z)$ is an estimate of the Hessian as in [55].

B Parallel reduction for norm-2 computation

Algorithm 4 Parallel Reduction to Compute $\|u\|^2$

Require: $u \in \mathbf{R}^n$, accessible to all threads in a block

Ensure: Scalar $\text{norm2} = \sum_{j=1}^n u_j^2$

```
1:
2: inline function _reduction_norm2(u, n)
3:     Allocate shared_mem[1 .. T] = 0 // T = threads per block
4:      $j \leftarrow \text{threadIdx.x}$ 
5:     while  $j \leq n$  then
6:         shared_mem[j]  $\leftarrow$  shared_mem[j] +  $u[j]^2$  // Julia is 1-indexed
7:     end
8:     _syncthreads()
9:
10: // Set  $s$  to the largest number of power 2 that is smaller than  $n$ 
11:      $s = \text{prevpow}(2, n - 1)$ 
12:     while  $s > 1$ 
13:         if ( $j \leq s$  &&  $j + s \leq n$ ) then
14:             shared_mem[j]  $\leftarrow$  shared_mem[j] + shared_mem[j + s]
15:         end if
16:         _syncthreads()
17:          $s \gg 1$  //Divide  $s$  by 2
18:     end for
19:     if  $j == 1$  then
20:         norm2  $\leftarrow$  shared_mem[1]
21:     end if
22: end
```

C Detailed benchmark results

Table 7: Solve times and iteration counts for the large OPF SOCP problem set

Problem	vars.	cons.	nnz(A)	nnz(P)	iterations				total time (s)			
					ClarabelGPU	Mosek*	ClarabelRs	Mosek	ClarabelGPU	Mosek*	ClarabelRs	Mosek
CASE2383WP_K	97600	20393	155950	0	110	-	107	-	1.48	-	2.79	-
CASE2383WP_K__API	97600	20393	155950	0	21	26	22	33	0.626	0.892	0.868	2.82
CASE2383WP_K__SAD	97600	20393	155950	0	96	-	97	-	1.12	-	2.94	-
CASE2312_GOC	98556	20518	159516	0	47	152	47	-	0.802	4.02	1.58	-
CASE2312_GOC__API	98556	20518	159516	0	65	244	64	-	1.04	6.15	1.71	-
CASE2312_GOC__SAD	98556	20518	159516	0	59	191	59	-	0.992	5.08	1.61	-
CASE2737SOP_K	109822	22777	176602	0	74	-	74	-	1.06	-	3.66	-
CASE2737SOP_K__API	109822	22777	176602	0	71	-	71	-	1.01	-	2.37	-
CASE2737SOP_K__SAD	109822	22777	176602	0	72	-	71	-	1.03	-	3.07	-
CASE2736SP_K	110022	22878	176901	0	69	-	74	-	1.24	-	2.15	-
CASE2736SP_K__API	110022	22878	176901	0	57	-	57	-	0.929	-	1.9	-
CASE2736SP_K__SAD	110022	22878	176901	0	72	-	72	-	1.01	-	4.2	-
CASE2746WP_K	111106	23320	178556	0	73	-	71	-	1.07	-	2.47	-
CASE2746WP_K__API	111106	23320	178556	0	33	35	-	34	0.76	1.26	-	2.24
CASE2746WP_K__SAD	111106	23320	178556	0	74	-	75	-	1.07	-	2.26	-
CASE2746WOP_K	111822	23434	179829	0	65	-	65	-	1	-	2.14	-
CASE2746WOP_K__API	111822	23434	179829	0	28	31	25	36	0.913	1.16	1.22	2.44
CASE2746WOP_K__SAD	111822	23434	179829	0	64	-	62	-	0.966	-	1.97	-
CASE3012WP_K	120676	25202	193907	0	86	-	89	-	1.16	-	5.32	-
CASE3012WP_K__API	120676	25202	193907	0	28	57	-	34	0.77	2.1	-	2.38
CASE3012WP_K__SAD	120676	25202	193907	0	99	-	94	-	1.31	-	2.86	-
CASE2848_RTE	122708	25858	197228	0	81	-	81	-	1.3	-	3.4	-
CASE2848_RTE__API	122708	25858	197228	0	76	218	75	-	1.35	6.1	3.7	-
CASE2848_RTE__SAD	122708	25858	197228	0	70	217	70	-	1.25	6	3.23	-
CASE2868_RTE	123912	26164	198869	0	84	228	86	-	1.41	6.72	8.48	-
CASE2868_RTE__API	123912	26164	198869	0	72	258	77	-	1.55	7.62	3.84	-
CASE2868_RTE__SAD	123912	26164	198869	0	79	287	79	-	1.32	8.18	6.56	-
CASE3120SP_K	124354	25856	199827	0	82	-	95	-	1.21	-	4.85	-
CASE3120SP_K__API	124354	25856	199827	0	96	-	93	-	1.32	-	5.08	-
CASE2853_SDET	128886	27445	206896	0	103	-	105	-	1.29	-	6.31	-
CASE2853_SDET__API	128886	27445	206896	0	120	-	116	-	1.41	-	3.45	-
CASE2853_SDET__SAD	128886	27445	206896	0	102	278	102	-	1.27	8.68	3.01	-
CASE3022_GOC	134780	28060	217434	0	41	176	-	140	0.984	5.86	-	9.95
CASE3022_GOC__API	134780	28060	217434	0	55	203	54	170	1.1	6.8	2.2	12.3
CASE3022_GOC__SAD	134780	28060	217434	0	41	177	41	141	0.971	5.76	1.74	9.79
CASE3375WP_K	139126	29112	223999	0	86	-	85	-	1.26	-	3.05	-
CASE3375WP_K__API	139126	29112	223999	0	161	-	147	-	1.86	-	4.82	-
CASE3375WP_K__SAD	139126	29112	223999	0	104	-	93	-	1.4	-	3.48	-
CASE2869_PEGASE	143608	30153	236217	0	53	236	53	-	1.25	8.46	4.9	-
CASE2869_PEGASE__API	143608	30153	236217	0	50	262	50	-	1.24	9.31	6.44	-
CASE2869_PEGASE__SAD	143608	30153	236217	0	48	278	48	-	1.22	9.66	2.99	-
CASE2742_GOC	144110	29856	236467	0	109	118	113	-	2.31	4.81	14.4	-
CASE2742_GOC__API	144110	29856	236467	0	101	128	103	-	2.15	5.06	7.2	-
CASE2742_GOC__SAD	144110	29856	236467	0	106	118	108	-	2.32	4.67	7.47	-
CASE4661_SDET	198498	41599	320728	0	139	-	140	-	2.7	-	16.8	-
CASE4661_SDET__API	198498	41599	320728	0	126	-	124	-	2.59	-	10.7	-

Table 7: Solve times and iteration counts for the large OPF SOCP problem set

Problem	vars.	cons.	nnz(A)	nnz(P)	iterations				total time (s)			
					ClarabelGPU	Mosek*	ClarabelRs	Mosek	ClarabelGPU	Mosek*	ClarabelRs	Mosek
CASE4661_SDET__SAD	198498	41599	320728	0	140	322	138	-	2.71	18.6	8.3	-
CASE3970_GOC	205819	42789	337328	0	140	156	139	-	3.79	9.51	12	-
CASE3970_GOC__API	205819	42789	337328	0	114	137	116	-	3.59	8.41	12.3	-
CASE3970_GOC__SAD	205819	42789	337328	0	147	168	141	-	3.23	10.2	12	-
CASE4020_GOC	216455	44877	355706	0	187	-	180	-	4.64	-	18.3	-
CASE4020_GOC__API	216455	44877	355706	0	98	142	101	-	3.13	8.86	21.7	-
CASE4020_GOC__SAD	216455	44877	355706	0	180	-	187	-	4.57	-	20.6	-
CASE4917_GOC	218213	45522	352833	0	52	166	52	147	1.7	8.82	4.82	16.5
CASE4917_GOC__API	218213	45522	352833	0	62	256	62	-	1.86	13.4	5.98	-
CASE4917_GOC__SAD	218213	45522	352833	0	48	183	-	169	1.69	9.8	-	18.7
CASE4601_GOC	225588	46885	368445	0	180	192	180	-	3.84	11.7	19.8	-
CASE4601_GOC__API	225588	46885	368445	0	109	148	109	156	3.03	8.96	14.4	19.3
CASE4601_GOC__SAD	225588	46885	368445	0	179	191	178	-	4.56	12.2	15	-
CASE4837_GOC	240160	49855	392884	0	134	154	138	-	3.82	10.3	36.1	-
CASE4837_GOC__API	240160	49855	392884	0	123	177	123	-	3.73	12.1	13.7	-
CASE4837_GOC__SAD	240160	49855	392884	0	133	162	131	-	3.88	11	17.5	-
CASE4619_GOC	254753	52616	419210	0	147	151	145	160	4.51	10.7	19.9	22.2
CASE4619_GOC__API	254753	52616	419210	0	129	161	131	-	4.01	11.7	15.8	-
CASE4619_GOC__SAD	254753	52616	419210	0	148	151	150	-	5.15	11	19.2	-
CASE5658_EPIGRIDS	282180	58620	461724	0	146	177	143	-	5.53	12.9	19.7	-
CASE5658_EPIGRIDS__API	282180	58620	461724	0	163	203	162	-	5.45	14.6	25.3	-
CASE5658_EPIGRIDS__SAD	282180	58620	461724	0	163	217	157	-	4.8	15.7	20.4	-
CASE6468_RTE	286248	59396	463599	0	103	250	98	-	3.01	15.8	12.4	-
CASE6468_RTE__API	286248	59396	463599	0	88	-	90	-	3.59	-	15.2	-
CASE6468_RTE__SAD	286248	59396	463599	0	98	255	99	-	3.08	16.4	19.7	-
CASE6470_RTE	287806	60144	465757	0	113	321	111	-	3.29	20.5	26.4	-
CASE6470_RTE__API	287806	60144	465757	0	85	327	85	-	2.95	21.1	15.5	-
CASE6470_RTE__SAD	287806	60144	465757	0	104	354	100	-	3.66	22.2	14.4	-
CASE6495_RTE	288050	60099	465939	0	114	323	114	-	3.37	20.4	16.4	-
CASE6495_RTE__API	288050	60099	465939	0	-	343	98	-	-	21.4	12.4	-
CASE6495_RTE__SAD	288050	60099	465939	0	112	344	108	-	3.25	22.1	25.2	-
CASE6515_RTE	288710	60239	466922	0	97	294	95	-	3.19	18.3	12.6	-
CASE6515_RTE__API	288710	60239	466922	0	85	341	81	-	2.97	21.4	21.4	-
CASE6515_RTE__SAD	288710	60239	466922	0	84	324	88	-	2.79	20.4	12.1	-
CASE7336_EPIGRIDS	358450	74618	585766	0	155	195	153	-	6.51	17.2	35.9	-
CASE7336_EPIGRIDS__API	358450	74618	585766	0	152	206	151	-	6.1	18.4	32.8	-
CASE7336_EPIGRIDS__SAD	358450	74618	585766	0	156	188	156	-	6.56	17.8	58.6	-
CASE10000_GOC	440997	92799	712177	0	71	87	-	-	3.58	9.49	-	-
CASE10000_GOC__API	440997	92799	712177	0	62	205	63	-	3.97	20.4	15.6	-
CASE10000_GOC__SAD	440997	92799	712177	0	89	152	-	-	4.13	16	-	-
CASE8387_PEGASE	459046	96351	750588	0	137	-	138	-	4.8	-	22.3	-
CASE8387_PEGASE__API	459046	96351	750588	0	141	-	141	-	5.08	-	25.9	-
CASE8387_PEGASE__SAD	459046	96351	750588	0	-	-	142	-	-	-	34.9	-
CASE9591_GOC	495073	102120	811889	0	229	206	226	-	12	32.7	69.9	-
CASE9591_GOC__API	495073	102120	811889	0	149	162	149	190	7.92	26.3	41.6	49.3
CASE9591_GOC__SAD	495073	102120	811889	0	230	-	227	-	10.8	-	78.6	-

Table 7: Solve times and iteration counts for the large OPF SOCP problem set

Problem	vars.	cons.	nnz(A)	nnz(P)	iterations				total time (s)			
					ClarabelGPU	Mosek*	ClarabelRs	Mosek	ClarabelGPU	Mosek*	ClarabelRs	Mosek
CASE9241_PEGASE	502110	104741	827419	0	72	-	67	-	5.29	-	14.9	-
CASE9241_PEGASE__API	502110	104741	827419	0	69	-	-	-	4.02	-	-	-
CASE9241_PEGASE__SAD	502110	104741	827419	0	72	-	68	-	4.26	-	21.7	-
CASE10192_EPIGRIDS	529695	109758	866501	0	94	113	95	-	5.74	16.5	29.5	-
CASE10192_EPIGRIDS__API	529695	109758	866501	0	93	115	-	-	5.92	16.7	-	-
CASE10192_EPIGRIDS__SAD	529695	109758	866501	0	110	-	114	-	6.36	-	33.2	-
CASE10480_GOC	573754	118760	943278	0	160	235	161	-	9.62	42.4	53.5	-
CASE10480_GOC__API	573754	118760	943278	0	139	213	-	-	8.91	39.3	-	-
CASE10480_GOC__SAD	573754	118760	943278	0	162	-	164	-	11	-	54.3	-
CASE13659_PEGASE	662910	140961	1081042	0	80	-	82	-	6.53	-	30.8	-
CASE13659_PEGASE__API	662910	140961	1081042	0	78	-	78	-	6.35	-	29.2	-
CASE13659_PEGASE__SAD	662910	140961	1081042	0	78	331	77	-	6.29	59.7	30.5	-
CASE20758_EPIGRIDS	1048059	218151	1709288	0	123	-	-	-	12.4	-	-	-
CASE20758_EPIGRIDS__API	1048059	218151	1709288	0	153	-	150	-	16	-	112	-
CASE20758_EPIGRIDS__SAD	1048059	218151	1709288	0	136	-	136	-	15.6	-	79.9	-
CASE19402_GOC	1064421	219911	1753874	0	259	-	254	-	21.8	-	168	-
CASE19402_GOC__API	1064421	219911	1753874	0	215	-	215	-	19.3	-	165	-
CASE19402_GOC__SAD	1064421	219911	1753874	0	253	-	253	-	21.5	-	175	-
CASE30000_GOC__API	1195834	249462	1921390	0	146	-	-	-	13.1	-	-	-
CASE24464_GOC	1202964	248644	1983519	0	233	-	219	-	21.2	-	133	-
CASE24464_GOC__API	1202964	248644	1983519	0	227	-	210	-	16.9	-	108	-
CASE24464_GOC__SAD	1202964	248644	1983519	0	226	-	221	-	17.9	-	124	-
CASE78484_EPIGRIDS	3904758	811998	6389202	0	413	-	410	-	118	-	1.02e+03	-
CASE78484_EPIGRIDS__API	3904758	811998	6389202	0	396	-	-	-	138	-	-	-
CASE78484_EPIGRIDS__SAD	3904758	811998	6389202	0	405	-	405	-	103	-	981	-